J. Fluid Mech. (2006), *vol.* 568, *pp.* 193–202.
doi:10.1017/S0022112006002734 Printed in the United Kingdom

Intrusive gravity currents

By M. R. FLYNN AND P. F. LINDEN

Department of Mechanical and Aerospace Engineering, University of California – San Diego, 9500 Gilman Drive, La Jolla, CA 92093-0411, USA

(Received 5 May 2006 and in revised form 1 August 2006)

The speed of a fluid intrusion propagating along a sharp density interface is predicted using conservation of mass, momentum and energy. For the special case in which the intrusion density equals the depth-weighted mean density of the upper and lower layers, the theory of Holyer & Huppert (*J. Fluid Mech.*, vol. 100, 1980, p. 739) predicts that the intrusion occupies one-half the total depth, its speed is one-half the interfacial long-wave speed and the interface ahead of the intrusion remains undisturbed. For all other intrusion densities, the interface is deflected vertically by a long wave that travels ahead of the intrusion and thereby changes the local upstream conditions. In these cases, the conservation equations must be matched to an exact solution of the two-layer shallow water equations, which describe the spatial evolution of the nonlinear wave. We obtain predictions for the intrusion speed that match closely with experiments and numerical simulations, and with a global energy balance analysis by Cheong, Keunen & Linden (*J. Fluid Mech.*, vol. 552, 2006, p. 1). Since the latter does not explicitly include the energetics of the upstream wave, it is inferred that the energy carried by the wave is a small fraction of the intrusion energy. However, the new more detailed model also shows that the kinematic influence of the upstream wave in changing the level of the interface is a critical component of the flow that has previously been ignored.

1. Introduction

The oceans and atmosphere exhibit regions of rapid vertical density variation, such as the thermocline and tropopause. Consequently, horizontal density-driven flow along a sharp interface arises in a variety of natural settings (Simpson 1997). Such flows are commonly referred to as interfacial gravity currents or intrusions and have been the subject of extensive experimental investigations (Britter & Simpson 1981; Mehta, Sutherland & Kyba 2002; Lowe, Linden & Rottman 2002; Sutherland, Kyba & Flynn 2004; Cheong, Kuenen & Linden 2006). Each of these studies examines high-Reynolds number intrusions generated by lock releases – fluid of density ρ_i intermediate to that of the two layers is initially separated by a vertical lock gate. The intrusion is initiated by removing the gate vertically. We are concerned with the case where the motion is independent of the lock length and hence the intrusion dynamics are not influenced by finite-volume effects. It is observed that, consistent with dimensional analysis, the propagation speed, U, is a constant which depends upon ρ_i and the layer depths and densities. Deceleration will be observed only when the flow becomes self-similar, which occurs once reflected disturbances from the endwall overtake the intrusion head (Rottman & Simpson 1983; Bonnecaze, Huppert & Lister 1993).

A theoretical description of intrusions that satisfactorily predicts U over a broad range of parameter space remains incomplete. In particular, complications arise when

describing non-equilibrium flow for which the intrusion density, ρ_i, differs from the depth-weighted mean density, ρ_E, of the upper and lower layers. Energy arguments in the spirit of Yih (1965) suggest that the available potential energy of an equilibrium intrusion is a global minimum and consequently $U > U_E$ when $\rho_i \neq \rho_E$. More specifically, a quadratic departure from the equilibrium solution is predicted, which shows good agreement with related experiments and (two-dimensional) direct numerical simulations (Cheong *et al.* 2006). However, this energy-conserving approach is based on the assumption that the leading-order behaviour of non-equilibrium intrusions may be recovered by judicious interpolation of three well-known flows, namely heavy and light gravity currents and the equilibrium intrusion. Therefore, although the assumptions applied by Cheong *et al.* (2006) provide a model in good agreement with experiments, they remain to be justified by a more rigorous examination of non-equilibrium flow that includes some quantitative description of the various forces at play.

The foundations of such an analysis were established in the earlier work of Holyer & Huppert (1980) who extended the gravity-current study of Benjamin (1968) by considering mass, momentum and energy conservation in a control volume moving with the intrusion head. In the equilibrium case, Holyer & Huppert's analysis accurately predicts the intrusion speed, U. However, when $\rho_i \neq \rho_E$, there are significant discrepancies between the predicted and observed speeds (Sutherland *et al.* 2004). Here, we show that these discrepancies are due to the observed upstream deflection of the interface that is caused by a long wave propagating ahead of the intrusion. Although Holyer & Huppert (1980) considered the possibility of downstream wave propagation (i.e. a stationary wave train behind the intrusion head), this upstream deflection is not accounted for in their theory and consequently, in many circumstances, the upstream conditions assumed in their calculations do not apply. In this paper we include the effect of the upstream wave explicitly and calculate the intrusion speed for non-equilibrium intrusions. Whereas the outcome of this analysis produces results similar to those of Cheong *et al.* (2006), these approaches are nonetheless fundamentally distinct as the latter is a simple energy balance in the spirit of Yih's calculation for a gravity current produced by lock exchange i.e. entirely different balances are applied in deriving the respective governing equations.

2. Holyer & Huppert's theory

We consider an intrusion of density ρ_i propagating at constant speed U along an interface between upper and lower layers of respective depths H_U and H_L, as shown in figure 1. Upstream and downstream of the intrusion front, the flow is assumed horizontal such that the pressure p is hydrostatic. Therefore, along the vertical segment BC

$$p = \begin{cases} p_Q - g\,\rho_U\,z, & 0 < z < H_U, \\ p_Q - g\,\rho_L\,z, & -H_L < z < 0, \end{cases} \tag{2.1}$$

where ρ_U and ρ_L are, respectively, the densities of the upper and lower layers, g denotes gravitational acceleration, $z = 0$ corresponds to the height of the interface and p_Q is the pressure along the interface far upstream from the intrusion (figure 1). Similarly, along AD

$$p = \begin{cases} p_R - g\rho_i\,h_U - g\,\rho_U(z - h_U), & h_U < z < H_U, \\ p_R - g\rho_i\,z, & 0 < z < h_U, \\ p_R - g\rho_i\,z, & -h_L < z < 0, \\ p_R + g\rho_i\,h_L - g\rho_L\,(z + h_L), & -H_L < z < -h_L, \end{cases} \tag{2.2}$$

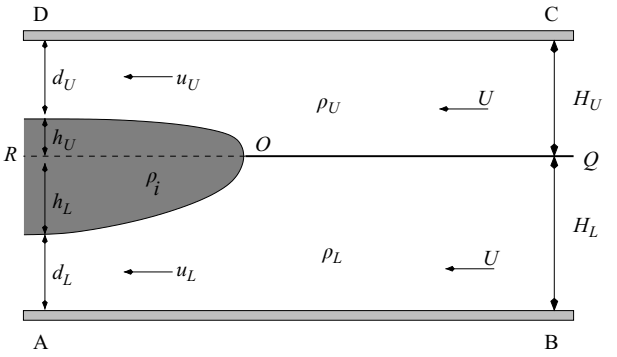

FIGURE 1. Definition sketch of an intrusion (shaded) and the control volume ABCD. The frame of reference is chosen so that the intrusion is at rest.

where h_U and h_L represent the vertical distances shown in figure 1. In this frame, all the fluid inside the intrusion is at rest. Hence $p_R = p_O$, the pressure of the stagnation point.

It is assumed that energy is conserved such that Bernoulli's equation may be applied along streamlines in the flow. Therefore, along the lower boundary of the intrusion downstream from the stagnation point†, we find

$$u_L^2 = 2g'_{Li}\, h_L = 2g'_{Li}\,(H_L - d_L), \tag{2.3}$$

where

$$g'_{Li} \equiv g\frac{\rho_L - \rho_i}{\rho_0}$$

is the reduced gravity of the intrusion and the lower layer and ρ_0 is a characteristic density. Similarly,

$$u_U^2 = 2g'_{iU}\, h_U = 2g'_{iU}\,(H_U - d_U), \qquad \text{where} \qquad g'_{iU} \equiv g\frac{\rho_i - \rho_U}{\rho_0}. \tag{2.4}$$

Here d_U and d_L are the layer depths specified in figure 1. Since the layer volume fluxes are constant, these depths are given by

$$d_U = \frac{U\,H_U}{u_U}, \qquad d_L = \frac{U\,H_L}{u_L}. \tag{2.5}$$

From (2.3), (2.4) and (2.5), conservation of mass therefore requires

$$g'_{iU}\frac{(H_U - d_U)\,d_U^2}{H_U^2} = g'_{Li}\frac{(H_L - d_L)\,d_L^2}{H_L^2}. \tag{2.6}$$

An independent relation for d_U and d_L is obtained via horizontal momentum conservation in the control volume ABCD. Because there are no externally imposed forces,

$$\int_A^D p + \rho u^2\,\mathrm{d}z = \int_B^C p + \rho u^2\,\mathrm{d}z. \tag{2.7}$$

† Strictly speaking, the stagnation point is deflected upwards by a distance $\zeta = U^2/2g$ relative to the interface (see (2.24) of Holyer & Huppert 1980). However, this elevation is negligible for most flows of practical interest. Consistent with the Boussinesq approximation and figure 1, therefore, we shall assume $\zeta \equiv 0$.

Using the hydrostatic pressure distributions (2.1) and (2.2) and the layer speeds given by (2.3) and (2.4), we find

$$\frac{p_O - p_Q}{\rho_0} H = g'_{iU} \left\{ \tfrac{1}{2}\left(H_U^2 - d_U^2\right) - \frac{2d_U}{H_U}(H_U - d_U)^2 \right\} + g'_{Li} \left\{ \tfrac{1}{2}\left(H_L^2 - d_L^2\right) - \frac{2d_L}{H_L}(H_L - d_L)^2 \right\}. \tag{2.8}$$

Applying Bernoulli's equation upstream along the interface, a second expression for $p_O - p_Q$ is obtained

$$\frac{p_O - p_Q}{\rho_0} H = g'_{iU} \frac{d_U^2}{H_U}(H_U - d_U) + g'_{Li} \frac{d_L^2}{H_L}(H_L - d_L). \tag{2.9}$$

Equating (2.8) and (2.9) gives

$$g'_{iU} \frac{(H_U - d_U)^2 (H_U - 2d_U)}{H_U} + g'_{Li} \frac{(H_L - d_L)^2 (H_L - 2d_L)}{H_L} = 0. \tag{2.10}$$

Equations (2.6) and (2.10) are, respectively, the Boussinesq limits of the mass and momentum conservation equations first derived for arbitrary density differences by Holyer & Huppert (1980) and written in this fashion by Sutherland *et al.* (2004). Although both equations are nonlinear in the dependent variables d_U and d_L, substantial simplification is possible for certain special cases, as we demonstrate in the following section.

3. Equilibrium intrusions

The easiest circumstance to consider is that of a doubly symmetric intrusion, for which $H_U = H_L$ and $\rho_i = \frac{1}{2}(\rho_L + \rho_U)$. This intrusion can be considered as two gravity currents, one above the interface and its mirror image below, travelling at the same speed, U (e.g. figure 7(*a*) of Lowe *et al.* 2002). In this case, $g'_{Li} = g'_{iU}$ and (2.6) is satisfied by $d_U = d_L = D$, say. Substituting this result in (2.10), we find two solutions: $D = \frac{1}{2}H$ and $D = \frac{1}{4}H$. The first solution corresponds to an intrusion with zero thickness, $h \equiv h_U + h_L = 0$, which, as in the bottom-propagating gravity current case, is the energy-conserving intrusion for infinitely deep layers $H_U = H_L \to \infty$. The second solution corresponds to $h = \frac{1}{2}H$, and is the energy-conserving half-depth solution described on p. 751 of Holyer & Huppert (1980).

This special case can be generalized to other instances in which the intrusion consists of two gravity currents that are, in effect, mirror images of one another. This equilibrium condition is realized whenever the intrusion is neutrally buoyant with respect to the undisturbed interface such that

$$g'_{iU} h_U = g'_{Li} h_L. \tag{3.1}$$

Equation (3.1), with (2.3) and (2.4), implies that the speeds u_L and u_U are equal. Thus

$$\frac{d_U}{H_U} = \frac{d_L}{H_L} \Rightarrow d_L + d_U = \tfrac{1}{2} H, \tag{3.2}$$

where conservation of mass and momentum has been applied. Hence an equilibrium intrusion occupies half the channel depth. Further, because (3.2) implies $h_U/H_U = h_L/H_L$, the neutral buoyancy condition (3.1) can be written as

$$\rho_i = \rho_E \equiv \frac{\rho_U H_U + \rho_L H_L}{H}. \tag{3.3}$$

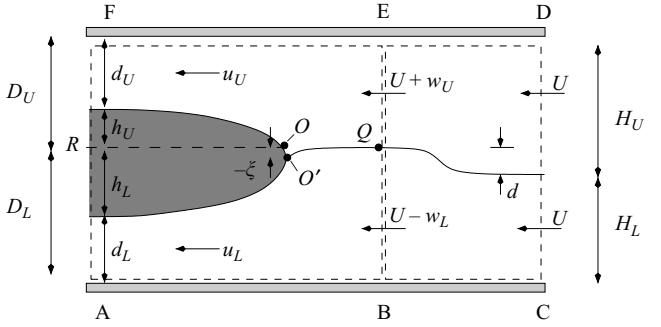

FIGURE 2. Propagation of a non-equilibrium intrusion in two-layer stratified media. For illustrative purposes, the intrusion depicted here has a density ρ_i that is larger than ρ_E, the depth-weighted mean density of the upper and lower layers. Thus the leading wave has positive amplitude, i.e. $d > 0$.

Thus when the intrusion density is the depth-weighted mean density ρ_E given by (3.3), a consistent solution to the mass, momentum and energy equations is found in which the interface remains undisturbed ahead of the intrusion (Sutherland *et al.* 2004). Note that (3.3) specifies either the equilibrium intrusion density ρ_E if the layer depths and densities are given or, if the intrusion and both layer densities are given, the equilibrium interface height h_E defined by

$$\frac{h_E}{H} = \frac{g'_{iU}}{g'_{LU}}, \tag{3.4}$$

where $g'_{LU} = g'_{iU} + g'_{Li}$ is the reduced gravity of the interface. Moreover, since $h_L + h_U = \frac{1}{2}H$, some simple manipulation shows that

$$h_L = \frac{h_E}{2}, \quad h_U = \frac{H - h_E}{2}. \tag{3.5}$$

Finally, the intrusion speed can be determined from (2.3) and (2.5):

$$U_E = \tfrac{1}{2}\sqrt{g'_{LU}\frac{h_E(H - h_E)}{H}}. \tag{3.6}$$

This result is in good agreement with the equilibrium experiments and simulations reported in Cheong *et al.* (2006) – see their figure 5. Nonetheless, (3.6) requires substantial modification for the case of non-equilibrium flow for which the stagnation point is deflected vertically by a long wave that travels ahead of the intrusion. As we illustrate in § 4, this necessitates an explicit coupling of intrusion and wave dynamics.

4. Non-equilibrium intrusions

The flow domain is divided into two control volumes as illustrated in figure 2. Control volume ABEF encompasses the (steady) intrusion, which is assumed stationary relative to the oncoming flow. Conversely, control volume BCDE encompasses the (nonlinear) wave of amplitude d, which propagates upstream at a velocity $c - U > 0$ (in the shifted reference frame).

4.1. *Intrusion*

Owing to wave-induced shear, the velocities of the upper and lower layers are different and are given, respectively, by $U+w_U$ and $U-w_L$ where w_U and w_L denote perturbations to the uniform upstream flow field considered in § 2. This disparity leads to an interfacial deflection $-\xi$ near the stagnation point O' where

$$\xi = \frac{(U+w_U)^2-(U-w_L)^2}{2g'_{LU}}. \tag{4.1}$$

Although the flow is Boussinesq, this displacement will be appreciable if $\rho_i \not\approx \rho_E$. In general, therefore, $|\xi| \not\ll h_U, h_L$ and by Bernoulli's equation

$$u_U = \sqrt{2g'_{iU}\,(D_U - d_U + \xi)}\,, \quad u_L = \sqrt{2g'_{Li}\,(D_L - d_L - \xi)}\,, \tag{4.2}$$

where $D_U = H_U - d$ and $D_L = H_L + d$ denote, respectively, the perturbed upper and lower layer depths (figure 2). Applying these results to the mass conservation equations for the upper and lower layers yields

$$U + w_U = \frac{d_U}{D_U}\sqrt{2g'_{iU}\,(D_U - d_U + \xi)}, \tag{4.3}$$

and

$$U - w_L = \frac{d_L}{D_L}\sqrt{2g'_{Li}(D_L - d_L - \xi)}, \tag{4.4}$$

respectively. By combining these results with (4.1), ξ can be expressed entirely in terms of the distances d_U, d_L, D_U and D_L and the reduced gravities g'_{iU}, g'_{Li} and g'_{LU}:

$$\xi = \frac{\dfrac{g'_{iU}}{g'_{LU}}\dfrac{d_U^2}{D_U^2}(D_U - d_U) - \dfrac{g'_{Li}}{g'_{LU}}\dfrac{d_L^2}{D_L^2}(D_L - d_L)}{1 - \dfrac{g'_{iU}}{g'_{LU}}\dfrac{d_U^2}{D_U^2} - \dfrac{g'_{Li}}{g'_{LU}}\dfrac{d_L^2}{D_L^2}}. \tag{4.5}$$

Furthermore, taking the difference between (4.3) and (4.4) and eliminating the wave-induced velocity w_L of the lower layer, yields

$$\frac{w_U\,H}{D_L} = \frac{d_U}{D_U}\sqrt{2g'_{iU}(D_U - d_U + \xi)} - \frac{d_L}{D_L}\sqrt{2g'_{Li}\,(D_L - d_L - \xi)}. \tag{4.6}$$

As expected from the previous discussion, horizontal momentum is conserved in the control volume ABEF and following the analysis given in § 2,

$$\begin{aligned}\frac{p_O - p_Q}{\rho_0}H = {} & g'_{iU}\left\{\tfrac{1}{2}\left(D_U^2 - d_U^2\right) - \frac{2d_U}{D_U}(D_U - d_U)^2\left[1 + \frac{\xi}{D_U - d_U}\right]\right\} \\ & + g'_{Li}\left\{\tfrac{1}{2}\left(D_L^2 - d_L^2\right) - \frac{2d_L}{D_L}(D_L - d_L)^2\left[1 - \frac{\xi}{D_L - d_L}\right]\right\}.\end{aligned} \tag{4.7}$$

Moreover, the pressure difference $p_O - p_Q$ can again be determined by applying Bernoulli's equation upstream along the interface whereby

$$\frac{p_O - p_Q}{\rho_0} = \frac{g'_{iU}g'_{Li}}{g'_{LU}}\left[\frac{d_U^2}{D_U^2}(D_U - d_U + \xi) + \frac{d_L^2}{D_L^2}(D_L - d_L - \xi)\right]. \tag{4.8}$$

Combining (4.7) and (4.8) yields the momentum balance

$$\frac{H g'_{iU} g'_{Li}}{g'_{LU}} \left[\frac{d_U^2}{D_U^2}(D_U - d_U + \xi) + \frac{d_L^2}{D_L^2}(D_L - d_L - \xi) \right] = g'_{iU} \left\{ \tfrac{1}{2}\left(D_U^2 - d_U^2\right) - \frac{2d_U}{D_U}(D_U - d_U)^2 \left[1 + \frac{\xi}{D_U - d_U} \right] \right\} + g'_{Li} \left\{ \tfrac{1}{2}\left(D_L^2 - d_L^2\right) - \frac{2d_L}{D_L}(D_L - d_L)^2 \left[1 - \frac{\xi}{D_L - d_L} \right] \right\}. \tag{4.9}$$

If the reduced gravities g'_{iU} and g'_{Li} and unperturbed layer depths $H_U = D_U + d$ and $H_L = D_L - d$ are known, (4.5), (4.6) and (4.9) represent three equations in the five unknowns ξ, w_U, d_U, d_L and d. To close the system, we now consider the behaviour of the upstream wave.

4.2. *Nonlinear wave*

The photographs presented in Sutherland *et al.* (2004) and Cheong *et al.* (2006) suggest that the upstream wave is non-undular and may have amplitude comparable with, or even greater than, the upper or lower layer depth. Motivated by these observations, we adopt a nonlinear dynamical description based on two-layer shallow water theory with a flat bottom boundary. Starting from the Euler equations and mass continuity, it can be shown that d and $v = -w_U H/D_L$ must satisfy the following coupled system of hyperbolic equations

$$\frac{\partial d}{\partial t} + \frac{\partial}{\partial x}\left[\frac{v(H_U - d)(H_L + d) - U H}{H} \right] = 0, \tag{4.10}$$

$$\frac{\partial v}{\partial t} + \frac{\partial}{\partial x}\left[g'_{LU} d + U v + \frac{v^2(H_U - H_L - 2d)}{2H} \right] = 0. \tag{4.11}$$

An exact solution to (4.10) and (4.11) is found in which the Riemann invariant

$$\sin^{-1}\left(\frac{D_L - D_U}{H} \right) - \sin^{-1}\left(\frac{w_U H}{D_L \sqrt{g'_{LU} H}} \right) = \sin^{-1}\left(\frac{D_L - D_U - 2d}{H} \right) \tag{4.12}$$

is conserved along characteristics (Baines 1995, § 3.3). Equation (4.12) relates the wave amplitude d to the wave-induced velocity w_U of the upper layer and can be expressed in equivalent algebraic form as follows

$$\sqrt{g'_{LU} H}\, D_L (D_L - D_U - 2d) = (D_L - D_U)\sqrt{g'_{LU} H D_L^2 - w_U^2 H^2} - w_U H \sqrt{H^2 - (D_L - D_U)^2}. \tag{4.13}$$

In the experiments of Cheong *et al.* (2006) the intrusion was generated by releasing intermediate-density fluid from a lock by removing a vertical barrier. The amplitude of the wave can be estimated by considering the vertical adjustment of the intrusion fluid as it is released from the lock. When ρ_i exceeds the depth-weighted mean density ρ_E, the intrusion will sink relative to the upstream interface and consequently over the time interval Δt, a volume of fluid

$$V = \Lambda(h_E - H_L) U \Delta t \tag{4.14}$$

is added to the lower layer. Here h_E is the equilibrium height defined by (3.4) and Λ is an unknown factor that characterizes the collapse of the intrusion fluid towards its level of neutral buoyancy. If this adjustment is static, $\Lambda = 1$, but we expect a smaller

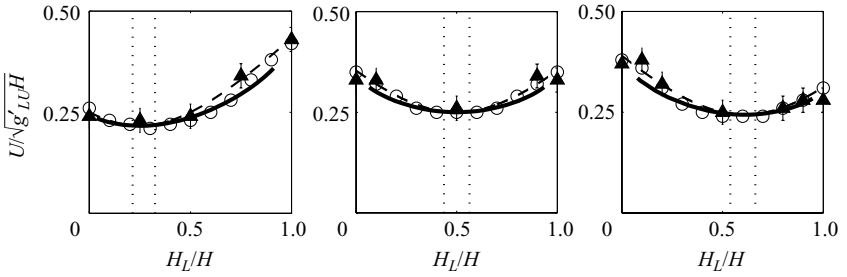

FIGURE 3. Intrusion speed as a function of the interface height for (*a*) $h_E/H = 0.25$, (*b*) $h_E/H = 0.50$ and (*c*) $h_E/H = 0.61$. Data points are taken from Cheong *et al.* (2006) and show the results of both experiments (triangles) and numerical simulations (circles). Solid and dashed curves are as indicated in the text. The vertical dotted lines show the range of validity of the model equations with $d \equiv 0$, i.e. a flat upstream interface.

value because dynamical effects are important. The addition of volume to the lower layer requires the dense fluid ahead of the intrusion to rise by an amount

$$d = \frac{V}{(c-U)\Delta t} = \Lambda(h_E - H_L)\frac{U}{c-U}. \tag{4.15}$$

For small d, c is approximately the linear long wave speed and by (3.6), $c \sim 2U$, whereby

$$d \sim \Lambda(h_E - H_L) = \Lambda\left(H\frac{g'_{iU}}{g'_{LU}} - H_L\right). \tag{4.16}$$

Experiments conducted by Cheong *et al.* (2006) confirm the validity of this leading-order approximation and give $\Lambda \simeq 0.3$. For this numerical value of Λ, we find an expected symmetry in H_L about $H_L/H = \frac{1}{2}$ when $g'_{iU} = g'_{Li}$, i.e. $h_E/H = \frac{1}{2}$ (see § 5).

The balances quantified by (4.5), (4.6), (4.9), (4.13) and (4.16) represent a closed system of equations for the unknowns ξ, w_U, d_U, d_L and d. By solving this system of equations, the intrusion speed U may be determined from (4.3).

5. Results

The governing equations are nonlinear and therefore multiple solutions are predicted for prescribed conditions. Here, attention is restricted to the solution for which the intrusion volume flux is maximized (Holyer & Huppert 1980; Faust & Plate 1984). As with the analysis of Holyer & Huppert (1980), this physical solution does not exist in all regions of parameter space. More specifically, model breakdown is likely to be encountered if the leading-order balance suggested by (4.16) proves inadequate, i.e. higher-order terms in $h_E - H_L$ become significant, or the upstream disturbance takes the form of a bore rather than a long wave of expansion. In contrast to earlier studies, however, the system of equations considered here yields a physically meaningful solution in a relatively broad neighbourhood of the equilibrium point $h_E = H_L$. For example, with $h_E/H = 0.5$, (4.5), (4.6), (4.9), (4.13) and (4.16) admit a physical solution for $H_L/H \simeq 0.0663$ to 0.934. By contrast if the wave amplitude d (and hence the velocities w_U and w_L) are set identically to zero, intrusion properties may be determined only over the restricted range $0.437 \lesssim H_L/H \lesssim 0.564$.

Figure 3 shows the intrusion speed (normalized by $\sqrt{g'_{LU}H}$) as a function of the non-dimensional interface height, H_L/H, for three choices of h_E/H. Solutions

predicted by the equations of §4 are indicated by the thick solid line. The dashed lines indicate the speeds obtained from the global energy-conserving model described in §4 of Cheong *et al.* (2006), which proposes the following relationship between U, H_L and h_E:

$$\frac{U}{\sqrt{g'_{LU}H}} = \tfrac{1}{2}\sqrt{\left(\frac{H_L}{H}\right)^2 - \frac{2H_L h_E}{H^2} + \frac{h_E}{H}}. \tag{5.1}$$

Although this result neglects the kinematic influence of the leading interfacial waves, strong qualitative agreement is observed between (5.1) and the detailed equations of §4. In particular, both models predict a global minimum of $U = U_E$ when $H_L = h_E$, in which case there is no mass transport across the vertical level $z = H_L$ during the gravitational adjustment of the intrusion. By contrast, when $H_L \neq h_E$ (i.e. $\rho_i \neq \rho_E$), intrusion fluid steadily rises or falls behind the intrusion front, which provides an additional source of energy to drive the flow (Cheong *et al.* 2006).

Quantitative differences between the solid and dashed lines of figure 3 elucidate the dynamic influence of the interfacial waves, which play a secondary, yet purely parasitic role. As is clear from figure 3(*a*) in particular, the lower estimates of the intrusion speed predicted by (4.5), (4.6), (4.9), (4.13) and (4.16) provide a closer fit with the results of the two-dimensional direct numerical simulation algorithm described in Cheong *et al.* (2006). Consistent with expectations, agreement is particularly strong as $H_L \to h_E$, where the leading-order approximation (4.16) is most appropriate.

6. Conclusions

A fluid intrusion necessarily excites an upstream interfacial wave when the intrusion density, ρ_i, differs from the depth-weighted mean density, ρ_E, of the upper and lower layers. In general, this disturbance will be nonlinear and will exert some non-trivial dynamical influence in that the wave (i) deflects the interface ahead of the intrusion and thereby alters the vertical position of the stagnation point, and, (ii) causes a shear such that the local horizontal velocities of the upper and lower layers are unequal. These effects may be incorporated into existing models by combining exact solutions of the two-layer shallow water equations with mass, momentum and energy conservation applied to a control volume surrounding the intrusion head. The coupled equations, which are given by (4.5), (4.6), (4.9), (4.13) and (4.16), provide good agreement with the results of analogue experiments and numerical simulations.

The analytical model developed herein also shows relatively strong agreement with the results of Cheong *et al.* (2006). In contrast to the present discussion, their formulation omits a detailed consideration of the force balance that provides the impetus for motion. Rather, using a Yih (1965)-type energy argument, non-equilibrium intrusions are described in terms of related equilibrium flows. The fact that these completely different approaches yield comparable results is encouraging and suggests that the upstream interfacial wave extracts only a small fraction of the intrusion kinetic energy, as has been observed in the case of vertically propagating internal waves by Ungarish & Huppert (2002) and Flynn & Sutherland (2004). This is different, however, from arguing that the interfacial wave has negligible impact. Indeed, as is suggested by figure 3, Benjamin (1968)-type models that fail to account for the upstream wave-induced effects summarized in the previous paragraph yield physically relevant solutions only over a limited region of parameter space.

Financial support was generously provided by NSERC (Canada), CMOS and NSF under Grant No. CTS-0209194. Engaging discussions with Drs L. Armi, S. B. Dalziel, J. W. Rottman and B. R. Sutherland are also acknowledged. Finally, the authors would like to thank three anonymous referees whose thoughtful remarks improved the quality of the present discussion.

REFERENCES

Baines, P. G. 1995 *Topographic Effects in Stratified Flows*. Cambridge University Press.

Benjamin, T. B. 1968 Gravity currents and related phenomena. *J. Fluid Mech.* **31**, 209–248.

Bonnecaze, R. T., Huppert, H. E. & Lister, J. R. 1993 Particle-driven gravity currents. *J. Fluid Mech.* **250**, 339–369.

Britter, R. E. & Simpson, J. E. 1981 A note on the structure of the head of an intrusive gravity current. *J. Fluid Mech.* **112**, 459–466.

Cheong, H.-B., Kuenen, J. J. P. & Linden, P. F. 2006 The front speed of intrusive gravity currents. *J. Fluid Mech.* **552**, 1–11.

Faust, K. M. & Plate, E. J. 1984 Experimental investigation of intrusive gravity currents entering stably stratified fluids. *J. Hydraul. Res.* **22**(5), 315–325.

Flynn, M. R. & Sutherland, B. R. 2004 Intrusive gravity currents and internal gravity wave generation in stratified fluid. *J. Fluid Mech.* **514**, 355–383.

Holyer, J. Y. & Huppert, H. E. 1980 Gravity currents entering a two-layer fluid. *J. Fluid. Mech.* **100**, 739–767.

Lowe, R. J., Linden, P. F. & Rottman, J. W. 2002 A laboratory study of the velocity structure in an intrusive gravity current. *J. Fluid Mech.* **456**, 33–48.

Mehta, A., Sutherland, B. R. & Kyba, P. J. 2002 Interfacial gravity currents: Part II – wave excitation. *Phys. Fluids* **14**, 3558–3569.

Rottman, J. W. & Simpson, J. E. 1983 Gravity currents produced by instantaneous releases of a heavy fluid in a rectangular channel. *J. Fluid Mech.* **135**, 95–110.

Simpson, J. E. 1997 *Gravity Currents*, 2nd Edn. Cambridge University Press.

Sutherland, B. R., Kyba, P. J. & Flynn, M. R. 2004 Intrusive gravity currents in two-layer fluids. *J. Fluid Mech.* **514**, 327–353.

Ungarish, M. & Huppert, H. E. 2002 On gravity currents propagating at the base of a stratified fluid. *J. Fluid Mech.* **458**, 283–301.

Yih, C. C. 1965 *Dynamics of Nonhomogeneous Fluids*. Macmillan.